Tailored Emulsion-templated Porous Polymer Scaffolds for iPSC-derived Human Neural Precursor Cell Culture

Ashley R. Murphy[a], Irene Ghobrial[b], Pegah Jamshidi[b], Andrew Laslett[c], Carmel M. O'Brien[c], Neil R. Cameron*[a,d]

[a] Department of Materials Science and Engineering, Monash University, 22 Alliance Lane, Clayton, VIC 3800, Australia. Email: neil.cameron@monash.edu

[b] Australian Regenerative Medicine Institute, Science, Technology, Research and Innovation Precinct (STRIP), Monash University, Clayton Campus, Wellington Road, Clayton, VIC 3800, Australia

[c] CSIRO Manufacturing, Research Way, Clayton, VIC 3168, Australia.

[d] School of Engineering, University of Warwick, Coventry, CV4 7AL, U.K.

Corresponding author: Prof Neil R. Cameron, Department of Materials Science and Engineering, Monash University, 22 Alliance Lane, Clayton, VIC 3800, Australia. T: +61 3 99020774; neil.cameron@monash.edu.

Abstract

The work here describes the synthesis of tailor-made, porous, polymeric materials with elastic moduli in the range associated with mammalian brain tissue (0.1-24 kPa). Three new emulsion-templated porous polymer materials (polyHIPEs) were synthesised by thiol-ene photopolymerisation from hexanediol diacrylate (HDDA) and polyethylene glycol diacrylate (PEGDA) crosslinkers and compared with a previously reported material prepared from trimethylolpropane triacrylate (TMPTA). The materials were found to have an average pore diameter of 30-63 μm and a porosity of 77% and above. PEGDA crosslinked materials at 80 and 85% porosity, when swollen in PBS at 37°C, were found to have an elastic modulus of 18 and 9.0 kPa respectively. PEGDA crosslinked materials were also found to have a swelling ratio of 700% in PBS at 37°C. PEGDA crosslinked materials had improved visible light transmission properties when compared to TMPTA crosslinked materials under a bright field microscope. All materials were shown via hematoxylin and eosin staining to support the infiltration and attachment of induced pluripotent stem cell (iPSC)-derived human neural progenitor cells (hNPCs). HNPCs on all materials were demonstrated in short term 3D cultures to maintain a phenotype consistent with early neural lineage specification via immunohistochemical staining for the intermediate filament protein vimentin.

Introduction

The human brain is the most complex and least understood organ of the human body. Key challenges for researchers, given rapidly aging populations in developed countries, are not only understanding how neurological diseases develop, but also how to stop their progression. A plethora of neurological disorders and diseases exist, yet little to no cures are apparent for many of these conditions. The limited access to live human neural tissue,[1] along with physiologically inaccurate 2D cell cultures[2] and questionably valid mouse models[3, 4] have made it difficult for researchers to study the human brain and human neurological disorders. Advances in this field require new tools with which to recreate human neural tissue *in vitro,* and produce representative, healthy tissue and disease models, for the study of neurological diseases and new therapeutic targets.

3D cell culture and tissue engineering techniques aim to produce cells and tissue that are physiologically comparable to those found *in vivo*. Cells receive a variety of cues from their surrounding environment including: the extracellular matrix (ECM), soluble factors and adjacent cells, which can influence cell behaviour. By designing tailor-made tissue engineering scaffolds that mimic as closely as possible the native ECM of the desired tissue-type, it is possible to grow tissue *in vitro* with greater physiological accuracy than current systems, which typically are flat, stiff 2D substrates. Biomaterials used as tissue engineering scaffolds come in a range of formats, but must generally be highly porous to allow cell infiltration and adequate nutrient/waste diffusion, have similar mechanical properties to the tissue of interest, be able to degrade at a suitable rate to non-toxic degradation products and be biocompatible.[5, 6]

Somatic stem cells exist in specifically defined microenvironments known as niches. These niches deliver specific extracellular cues typically in the form of cell-cell interactions, cell-factor interactions and cell-matrix interactions. Through these interactions the stem cell niche can support the self-renewal of stems cells as well as trigger the specific linage commitment of stem cells.[7] The neural stem cell niche is located primarily in the sub ventricular zone of the human brain, and provides the specific set of conditions for the maintenance of neural stem cells and the commitment of neural stem cells to neuronal and glial cell lineages for the growth of neural tissue.[8] The neural stem cell niche-ECM is comprised of a hyaluronic acid back bone[9] and proteins laminin, fibronectin, proteoglycans and other molecules.[10] When designing advanced *in vitro* environments for the creation of stem cell-derived tissue it is important to take design characteristics from the stem cell niche as much as possible.[11]

Access to live, developing human neural tissue is extremely limited due to the sensitivity and accessibility of the brain, therefore current research techniques take advantage of human pluripotent stem cells (hPSCs) and subsequent directed differentiation techniques. HPSCs obtained from human embryos,[12] human embryonic stem cells (hESCs), or derived from somatic cells,[13] induced pluripotent stem cells (iPSCs), have the ability to differentiate to all cell types in the human body. By specifically controlling *in vitro* environments, hPSC differentiation can be directed toward certain cell lineages to produce a variety of cell types. Human neural progenitor cells (hNPCs) can be quickly and efficiently generated from hPSCs via single[14-16] and dual SMAD pathway inhibition.[17] Techniques like these make it possible to study cells that are otherwise extremely difficult to gain access to *in vitro*.

It is important for tissue engineering scaffolds to mimic the mechanical properties of the tissue-type of interest. The mechanical properties of mammalian brain tissue have been widely studied via a variety of methods, including: mechanical testing in tension and compression;[18] dynamic mechanical analysis;[19] atomic force microscopy;[20] and indentation testing.[21] Tissue from a variety of species, including human, primate, porcine and rat has been studied. The elastic modulus of the mammalian brain can be broadly classified to be in the region 0.1-24 kPa[22, 23] depending on test methods, test conditions and species, as well as on age and development. When designing materials for neural tissue engineering it is important that their elastic modulus falls within this range. Scaffold stiffness has been shown to affect the ability of mouse embryonic and rat neural stem cells to attach, survive, proliferate and differentiate to neurons and glia on a range of different substrates.[24-27]

3D porous polymeric materials have shown promise as tissue engineering scaffolds.[28-31] Their high porosity and pore interconnectivity make them ideal scaffolds for highly interactive, networked 3D cell cultures.[32] Their porous nature allows for deeper and more uniform nutrient transport, as well as allowing cells to freely migrate throughout the structure with limited resistance. Polymerised high internal phase emulsions (PolyHIPEs) are a class of solid porous material that have been shown to be effective as tissue engineering scaffolds.[29, 33-44] They are produced by a process called emulsion templating in which the external phase of an emulsion is polymerised and the internal phase is vacated to leave a highly porous structure.[45-47] PolyHIPEs specifically are produced using an emulsion greater than 74% internal phase volume, of which is the minimum phase volume that ensures complete droplet packing of uniform droplet size.[48] This yields a highly porous structure of interconnected voids. In most cases, polyHIPEs are produced via thermally initiated radical polymerisation reactions. However, these reactions are relatively slow and require emulsions that

are sufficiently stable at polymerisation temperature (typically 50-70 ^{o}C), ruling out the use of certain monomers. More recently, photoinitiated thiol-ene click-chemistry reactions have been used to polymerise emulsions that lack long-term stability.[39, 49, 50] This broadens the range of monomers that can potentially be used for the synthesis of polyHIPE materials, in particular allowing the use of monomers that do not lead to highly stable emulsions.

The work presented here investigates the creation of thiol-ene polyHIPE materials with similar mechanical properties to that of mammalian brain tissue. The methods employed include reducing the crosslink density of the network polymer, increasing the distance between crosslinks in the network and increasing the overall porosity of the material. The mechanical properties of the materials produced were determined in tensile mode. The ability of materials to absorb medium was determined as well as degradability under biological and non-biological conditions. Finally, biocompatibility of materials was investigated by exploring their ability to support the adherence and short term expansion of hiPSC-derived neural progenitor cells.

Experimental

Materials

Trimethylolpropane triacrylate (TMPTA), trimethylolpropane tris(3-mercaptopropionate) (TMPTMP), 1,6-hexanediol diacrylate (HDDA), poly(ethylene glycol) diacrylate M_n=700 (PEGDA), diphenyl(2,4,6-trimethylbenzoyl)phosphine oxide/2-hydroxy-2-methylpropiophenone blend (photointiator), phosphate buffered saline (PBS), 1,2-dichloroethane and laminin from Engelbreth-Holm-Swarm murine sarcoma basement membrane were all purchased from Sigma-Aldrich. AggreWell^{TM}800 plates, Neurocult^{TM} NS-A Basal Medium (Human), Neurocult^{TM} NS-A Proliferation

Supplement, STEMdiff™ Neural Progenitor Medium (STEMdiff NPM), STEMdiff™ Neural Progenitor Freezing Medium (STEMdiff NPM Freeze Medium) and Y-27632 RHO/ROCK inhibitor were obtained from STEMCELL Technologies. Essential 8™ Medium, Geltrex LDEV-Free hESC-Qualified Reduced Growth Factor Basement Membrane Matrix, EDTA (0.5M) pH 8.0, TrypLE™ Express Enzyme (1X), DMEM/F12 (Ham) (1:1) + GlutaMAX™-I (1X) supplement (DMEM/F12), StemPro® Accutase® Cell Dissociation Reagent, Trypan Blue Stain, Goat anti-Rabbit IgG (H+L) Alexa Fluor® 568, 4',6-Diamidino-2-Phenylindole, Dihydrchloride (DAPI), Nunc™ Lab-Tek™ II 8-well Chamber Slides™ and Dulbecco's phosphate buffered saline without calcium and magnesium (DPBS) were all purchased from Life Technologies Australia Pty Ltd. HYPERMER™ B-246SF-LQ-(AP) was obtained from Croda. 3CB2 Anti-Vimentin IgM mouse antibody was purchased from Developmental Studies Hybridoma Bank. Recombinant human basic FGF (bFGF) and recombinant human EGF were purchased from PeproTech. Corning® Costar® Ultralow attachment multiwell plates were purchased from Corning. Recombinant Human Noggin protein was purchased from R&D Systems.

PolyHIPE Synthesis

The polyHIPE synthesis procedure was developed from the work of Lovelady *et al*.[49] A hydrophobic phase mixture consisting of TMPTMP, a multifunctional acrylate monomer (TMPTA, HDDA or PEGDA) (**Figure 1**), surfactant Hypermer B246 (3% w/w of hydrophobic phase) and photoinitiator (5% w/w of hydrophobic phase) was dissolved in dichloroethane (for amounts see **Table S1**). The mixture was added to a two-neck 250 ml round bottom flask and stirred at a defined speed (**Table S1**) using a D-shaped polytetrafluoroethylene (PTFE) overhead paddle stirrer (Sigma-Aldrich). A hydrophilic phase of MilliQ water was added to the mixture drop-wise at approximately 1 drop per second until all water was added. The mixture was then stirred for a further period of time (**Table S1**). The HIPE mixture was then poured into a cylindrical PTFE mould between two glass plates and

passed under a high intensity UV irradiator (Fusion UV Systems, Inc. Light Hammer® 6 UV curing system with an Heraeus belt conveyer) four times (twice on each side) at a power flux of 5 W/cm^2 and belt speed of 3.2 m/min. The resulting polyHIPE was washed in an immersion of acetone overnight. The polyHIPE was further washed by Soxhlet extraction using dichloromethane for 24 hours. The polyHIPE was air dried overnight then vacuum dried for 24 hours at room temperature. PolyHIPE materials produced by this method are known to contain residual thiols resulting from acrylate homopolymerisation that competes with thiol-acrylate reactions[51]. Residual thiol concentrations were measured by Ellman's assay and were found to range from 28-63 μmol/g (see Supplementary Information).

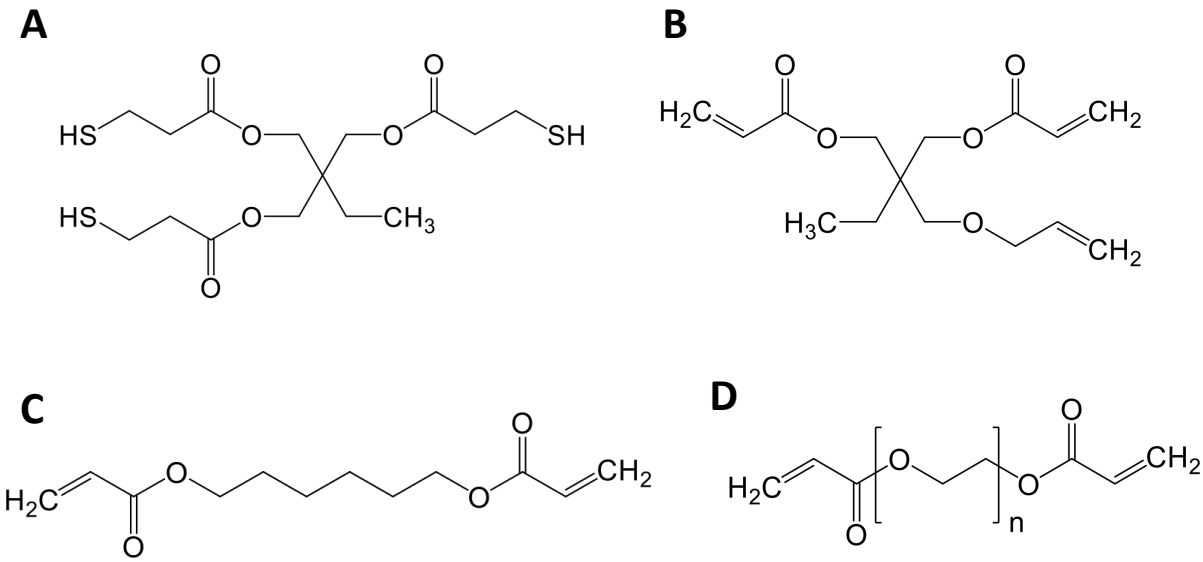

Figure 1. Monomers used in polyHIPE synthesis. Trimethylolpropane tris(3-mercaptopropionate) (**A**), trimethylolpropane triacrylate (**B**), 1,6-hexanediol diacrylate (**C**), and poly(ethylene glycol) diacrylate (n=13) (**D**).

Scanning Electron Microscopy

PolyHIPE structure was analysed using an FEI Nova NanoSEM 450 FEGSEM operating at 5 kV. Samples were mounted on aluminium stubs using carbon tape and sputter-coated with iridium.

Void sizes were measured using Image J imaging software by selecting 100 random voids across an image of 200x magnification. A statistical correction factor was used to account for underestimations of void sizes in the cross-sectional image.[52]

Helium Pycnometry

Skeletal density of polyHIPE materials was analysed using a Micrometrics AccuPyc II 1340 Gas Pycnometer. Experiments were performed using helium gas at a pressure of 150 kPa and a cup size of 10 cm^3. 10 measurements of each sample were made. Porosity was determined using the following expression (**Equation 1**):

$$Porosity\ (\%) = \left(1 - \frac{bulk\ density}{skeletal\ density}\right) \times 100 \quad [1]$$

Mechanical Testing of Dry Samples

PolyHIPE samples were tensile tested to ASTMD638 standards. PolyHIPE materials were made in sheets approximately 3 mm thick. Dumbbell-shaped samples were then stamped out of the sheet using an ASTMD638 Type V die. Samples were tensile tested using an Instron 5848 MicroTester with Bluehill® software. Samples were tensile loaded uniaxially at a constant extension rate of 10 mm/min until break.

In situ Mechanical Testing

PolyHIPE samples were tensile tested under mimicked biological conditions in phosphate buffered saline at 37°C using a Bose Electroforce 3200 II *in situ* biomechanical tester with WinTest® 7 software. Samples were placed in a chamber of PBS recirculating at 37°C. Samples were then loaded uniaxially at a constant extension rate of 10 mm/min to the extension limits of the apparatus.

Analysis of Stress-Strain data

All stress-stain data obtained from these materials exhibited distinct non-linear J-shaped curves. The elastic modulus was deduced from these curves using a method described by Kendall and Fuller.[53] Briefly, the data was fit with the following power equation (**Equation 2**):

$$\sigma = \varepsilon\epsilon^{n} \quad [2]$$

Where σ is the nominal stress (force/original cross sectional area), ϵ is the nominal strain (change in length/original length) and ε is a constant corresponding to Young's modulus.

Swelling Experiments

Samples were dried in a vacuum oven until constant mass was reached (m_d). Rectangular samples of dimensions 3x5x5 mm were submerged in 15 ml PBS and incubated at 37°C for up to 2 hours. At different time intervals samples were removed from solution. The wet weight (m_w) was immediately measured. Samples were then pressed between two pieces of paper towel to vacate any PBS in pores and swollen weight (m_{sw}) was then determined. Two calculations were performed (**Equations 3-4)**:

$$Fluid\ uptake\ of\ whole\ scaffold\ (\%) = \frac{m_w - m_d}{m_d} \times 100 \quad [3]$$

$$Fluid\ uptkae\ of\ scaffold\ material\ (\%) = \frac{m_{sw} - m_d}{m_d} \times 100 \quad [4]$$

Degradation Experiments

Clean, dry, rectangular polyHIPE samples of dimensions 3x10x10 mm and known weight (m_i) were placed in 15 ml of PBS in Teflon™ capped vials at 37°C on orbital rotation at 70 rpm. After different time intervals up to 77 days, samples were removed from solution, washed three times with water, vacuum dried to constant mass and weighed (m_f). Percentage mass loss was calculated (**Equation 5**). Accelerated degradation experiments were performed to the exact same conditions with 0.1 M NaOH, at room temperature, instead of PBS.

$$Percentage\ mass\ loss\ (\%) = \frac{m_i - m_f}{m_i} \times 100 \qquad [5]$$

Cell culture

All work using hPSCs and derivative NPCs was carried out in accordance with Australia's National Health and Medical Research Council (NHMRC) National Statement on Ethical Conduct in Human Research (2007, updated 2015), the Australian Code of Responsible Conduct of Research (2007) and with approvals from Monash University and the CSIRO Human Research Ethics Offices.

The iPS cell line HDF51i-509, previously derived by Sendai reprogramming of human dermal fibroblast (HDF) cells,[54] was kindly provided under materials transfer agreement by Prof. Jeanne Loring (The Scripps Research Institute, CA, USA). HDF51i-509 hiPSCs were maintained in Essential 8™ (E8) medium on Geltrex™-coated tissue culture polystyrene at 37°C in an atmosphere containing 5% CO_2 and passaged using 0.5 mM EDTA.[55]

HiPSCs were directly differentiated *in vitro* to neural stem and progenitor precursor (NPC) cultures in serum-free culture via the initial formation of uniform-sized cell aggregate embryoid bodies

(EBs),[56] with neural lineage induction by bone morphogenic protein (BMP) inhibition in neurosphere suspension culture and subsequent monolayer mitogen expansion of generated NPCs.[14-16, 57, 58] Briefly, hiPSCs harvested from E8 maintenance culture with Accutase were seeded in AggreWell^{TM}800 plates at 10,000 cells/microwell (STEMCELL Technologies, as per manufacturer's protocol) in serum-free NeuroCult^{TM} NS-A human Basal Medium supplemented with NeuroCult^{TM} NS-A human Proliferation Supplement, 20 ng/µl recombinant human bFGF and 20 ng/µl recombinant human EGF, (Complete NeuroCult NS-A Proliferation medium), with the addition of 500 ng/ml human noggin and 10 µM ROCK inhibitor Y-27632.[59] AggreWell cultures were incubated undisturbed for 24-36 hours at 37°C/5% CO_2 before commencing partial daily media changes of Complete NeuroCult NS-A Proliferation medium supplemented with 500 ng/ml noggin. EBs were transferred after 5 days from AggreWell^{TM} plates to ultra-low attachment 6-well (10 cm^2/well) plates for neurosphere induction using the same noggin-supplemented proliferation medium as above for a further 9 days, replenishing medium every 2 days.

Neurospheres were mechanically dissociated using TrypLE Express with 15-20 minute/37°C incubations and cells seeded at 5x10^4/cm^2 onto tissue culture wells coated with laminin (10 µg/ml in DMEM/F12, coating 1 µg/cm^2) in Complete NeuroCult NS-A Proliferation to generate an adherent monolayer culture of neural precursor cells. NPCs were passaged at ~80% confluence each 4-7 days using Accutase, replating at ~5-10x10^4 cells/cm^2 and transferring renewing stem cells to STEMdiff NPM from the third passage, with media changes each second day (as per STEMdiff Neural System protocols, STEMCELL Technologies). An established HDF51-509i NPC line was successfully maintained for up to 15 passages in STEMdiff NPM, cryopreserved in STEMdiff NPM Freeze Medium and thawed as an expanding population of NPCs, validated by immunocytochemical staining for Vimentin expression. HNPCs were routinely expanded on

laminin coated tissue cultureware in STEMdiff NPM for up to 10 passages prior to adaptation to scaffold test surfaces.

3D hNPC culture on scaffolds: circular disk scaffolds of 15 mm diameter and 200 µm thickness were cut from a cylinder of polyHIPE by sectioning using a Leica VT100 S vibrating-blade microtome. Samples too soft to section with a vibratome were embedded in optimum cutting temperature (OCT) medium and sectioned using a Leica CM3050-S Cryostat. Disks were then assembled into well inserts purchased from ReproCELL Europe Ltd and placed in 12-well cell culture plates (3.8 cm^2/well). Scaffolds were sterilised by submerging 4 mL/well of 70% v/v ethanol in water for 10 minutes. Scaffolds were then washed twice with 3.5 mL/well of DMEM/F12 for 5 minutes each wash. Scaffolds were coated in 3.5 mL/well of 10 µg/mL laminin in DMEM/F12 for 2 hours at room temperature. The laminin solution was aspirated and $1x10^6$ HDF51i-509 NPCs in 150 µL of STEMdiff NPM were place on top of the scaffold. Scaffolds were incubated at 37°C in an atmosphere of 5% CO_2 for 3 hours to allow cells to settle and attach to the material, after which an extra 3.5 mL of STEMdiff NPM was carefully added so as not to disturb cell attachment. STEMdiff NPM was then replenished every 1-2 days. Following 3 days of culture scaffolds were fixed in 10% neutral buffered formalin pH 7 for 10-15 minutes for histological analyses.

Histology and Staining

Fixed scaffolds were processed to remove water and infiltrate with wax. Samples underwent a four hour formalin processing program of 80% ethanol, xylene then paraffin on a Leica PELORIS Tissue Processor. Processed scaffolds were then embedded in paraffin wax and sectioned into 4 µm slices using a Rotary Microtome CUT 4060 (microTEC). Sections were then mounted on polylysine slides (Thermo Scientific) and air-dried overnight at room temperature. To stain,

samples were dewaxed in xylene and washed with ethanol and water. Samples were then stained in Harris's Haematoxylin for 5 min. Samples were then washed with water, quickly immersed in acid alcohol and again washed with water before counterstaining with Eosin for 5 min. Stained sections were then washed with ethanol, dehydrated with xylene and cover slipped. Samples were then imaged with an Olympus BX51 microscope in brightfield mode using a Nuance FX Multispectral Imaging System.

Immunocytochemistry

For immunocytochemical staining, sections were prepared as described above. Sections underwent heat induced epitope retrieval at 98°C for 30 minutes in a Dako Target Retrieval Solution, citrate pH 6 solution on a Dako PT Link Rinse Station. HNPCs cultured on 8-well glass chamber slides were fixed using 4% formaldehyde in PBS and did not undergo the epitope retrieval process. Samples were incubated with blocking buffer, 10% v/v normal goat serum in PBS (blocking buffer), for 1 hour at room temperature then incubated in 4.4 µg/mL 3CB2 Anti-Vimentin IgM mouse primary antibody in blocking buffer for 1 hour at room temperature. Samples were then washed three times in PBS for 5 minutes each with agitation then incubated in goat anti-rabbit IgG (H+L) Alexa Fluor® 568 secondary antibody (4 µg/mL (1:500) in blocking buffer) for 1 hour at room temperature. Samples were subsequently washed three times in PBS for 5 minutes each with agitation, then counterstained with DAPI (2 µg/ml or 1:500) and incubated for 5 minutes at room temperature. Finally, samples were washed in PBS for 5 minutes, cover slipped and imaged using a Leica SP8 confocal microscope equipped with a x40 water objective and running LAS AF software (Leica MicroSystems. Manheim, Germany).

Results and Discussion

PolyHIPE Synthesis and Analysis

The monomer trimethylolpropane tris(3-mercaptopropionate) (trithiol) was reacted with three different multifunctional acrylate crosslinkers: trimethylolpropane triacrylate (TMPTA), 1,6-hexanediol diacrylate (HDDA) and poly(ethylene glycol) diacrylate (PEGDA) to produce materials of varying cross-linking density and mechanical properties. In an attempt to reduce the elastic modulus of the materials to that of mammalian brain tissue, three approaches were taken: reducing the crosslink density, increasing the physical length of crosslinks and increasing the porosity of the material.

TMPTA polyHIPEs were successfully produced using conditions previously reported (**Figure 2A**, **Table S1)**.[39] Attempts to use the same set of conditions with the HDDA monomer gave an unstable emulsion, possibly due to the reduction in external phase viscosity. Stirrer speed was increased to 470 rpm, to reduce internal phase droplet size and give a HIPE of good stability that was able polymerise (**Figure 2B**). PolyHIPE then made with the PEGDA monomer under the original TMPTA conditions formed a highly stable, highly viscous HIPE. Whilst very stable this HIPE would not polymerise under UV light, possibly due to monomer density reducing light penetration into the HIPE, preventing polymerisation. Lowering the monomer concentration in the organic phase to 0.5 M gave an unstable emulsion. A monomer concentration of 0.79 M in the organic phase gave a stable emulsion that was able to polymerise and give a material with the expected polyHIPE morphology (**Figure 2C**). Emulsions stirred for an additional 120 minutes after the addition of the droplet phase gave materials of the most uniform pore diameter. Under the same conditions the PEGDA system formed a stable, polymerisable emulsion up to 85% aqueous phase volume fraction.

Beyond this volume fraction emulsions would invert and stable water-in-oil emulsions were not formed. All systems that successfully polymerised, once washed and dried, gave a spongy, white material of varying degrees of elasticity.

All materials were observed by SEM to have a porous structure as a result of vacated internal phase water droplets (**Figure 2A-D**). An interconnected porous network is created by internal phase droplets coming into contact with adjacent droplets, and can be seen in all materials. Some defects can be seen in the materials made with the PEGDA monomer (**Figure 2C and D**), particularly in the thin sections between interconnects. This can possibly be a result of strain put on the soft material via expansion and shrinkage during the washing and drying processes. However, these small defects visually had little effect on the bulk structure of the material.

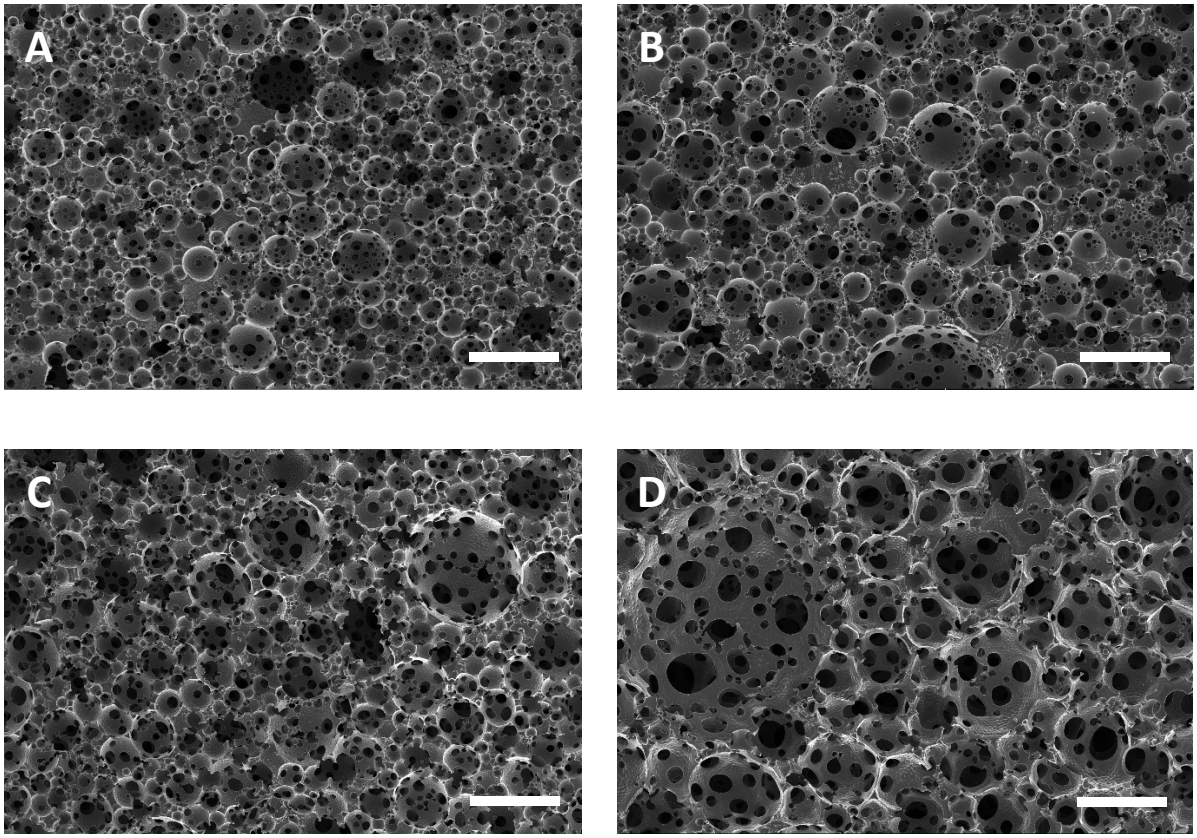

Figure 2. SEM images of polyHIPE materials synthesised with TMPTA crosslinker at 80% porosity (**A**), HDDA crosslinker at 80% porosity (**B**), PEGDA crosslinker at 80% porosity (**C**) and PEGDA crosslinker at 85% porosity (**D**). (Scale bar = 100 μm)

SEM images were analysed using Image J imaging software to determine pore diameter distributions (**Figure S1**) and averages (**Table S2**). A pore diameter between 20-70 μm has generally been shown to be ideal for the ingrowth and outgrowth of neurons within porous scaffolds.[60] The TMPTA polyHIPE material gave the lowest average pore diameter (30.3 ± 14.9 μm) and the narrowest pore size distribution (SD = 14.9 μm). Despite the increased stirring speed the HDDA polyHIPE gave a slightly larger average pore diameter (44.2 μm) than the TMPTA polyHIPE, most likely due to the change in external phase properties caused by the introduction of the HDDA monomer. The PEGDA polyHIPEs also had increased average pore diameters at the same stirrer speed compared to the TMPTA polyHIPE, possibly due to the increased water solubility of the PEGDA monomer which can promote emulsion coarsening. The 85% porous PEGDA polyHIPE had a higher average pore diameter (63.2 ± 31.5 μm) due to the increased internal phase volume of the emulsion.

PolyHIPEs, particularly the high porosity PEGDA polyHIPE, had a tendency to collapse if the pore diameter was too small or if the material was dried too quickly. It was therefore important to verify whether the porosity measured was the same as that expected from the emulsion internal volume fraction. Helium pycnometry was used to determine the skeletal density of the materials, which was then used to calculate the actual porosity (**Table S2**). All materials that were observed via SEM to have retained their porous structure were found to be within 4% of their desired formulated porosity.

Swelling Studies

Once synthesised, the polyHIPEs, in particular the PEGDA materials, were observed to swell significantly in polar organic solvents. Swelling studies were performed to quantify the swelling ability of all scaffold materials. The swelling ability of the scaffold as a whole (material and pores) and solely the material was quantified in PBS at 37°C (**Figure 3**).

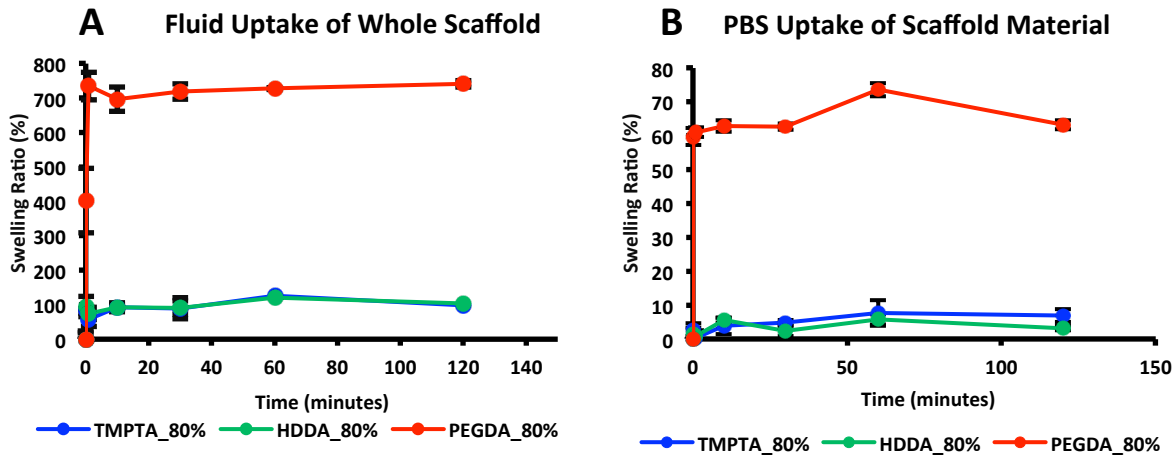

Figure 3. PBS uptake profiles of the scaffold material as a whole (**A**) and solely the scaffold polymer phase (**B**) (N=3, mean ± standard deviation)

All materials were expected to take up a certain amount of PBS due to their interconnected porous structure. Both TMPTA- and HDDA-based materials reached an equilibrium PBS uptake of around 100% of their weight after approximately 10 minutes (**Figure 3A**). The 80% porous PEGDA material was found to absorb more than seven times its own weight in PBS after 10 minutes swelling. The highly absorbing capacity of the PEGDA crosslinked materials is most likely due to the ethylene glycol backbone of the PEGDA crosslinker. These backbone units are able to interact

strongly with water through hydrogen bonding. Comparatively, the alkane backbone of the TMPTA and HDDA crosslinkers is quite hydrophobic, hence these materials take up less PBS. The PEGDA material itself (not accounting for pores) was also shown to be able to absorb around 60% its own weight in PBS, whilst the HDDA- and TMPTA-based materials only were shown to absorb around 5% of their weight. Again this follows the hypothesis that the more hydrophilic the backbone of the crosslinker the greater its ability to absorb PBS.

These results indicate that the PEGDA-crosslinked polyHIPEs display hydrogel-like properties in terms of their ability to absorb water. The PEGDA polyHIPE displays the characteristic of a hierarchical porosity, with pores due to the emulsion templating process and smaller pores present in the solid material itself which are able to absorb water. An ability to absorb a large amount of water translates into a better material environment for cell culture. Materials that can absorb more medium allow for cells to exist in a more nutrient-rich environment inside the scaffold. This could have an effect on the growth characteristics of cells inside the material.

Optical Properties

One of the major drawbacks of porous materials used as tissue engineering scaffolds is their poor optical properties. The opacity of solid porous polymers makes it very difficult to visualise live cells during culture using conventional microscopic techniques. PEGDA polyHIPEs, which were shown to have hydrogel-like properties due to the presence of a hydrophilic crosslinker, have significantly enhanced light transmission properties. Due to the high water content of these materials they are far more transparent than both the TMPTA- and HDDA-crosslinked materials. As can be seen in **Figure 4A** the PEGDA polyHIPEs are visibly more transparent than those for TMPTA. Further, under a bright field microscope (**Figure 4Bi-ii**) far better resolution is observed due to the increased

amount of light that is able to pass through the material. This increases the likelihood of live cell visualisation during cell culture using conventional microscopic techniques.

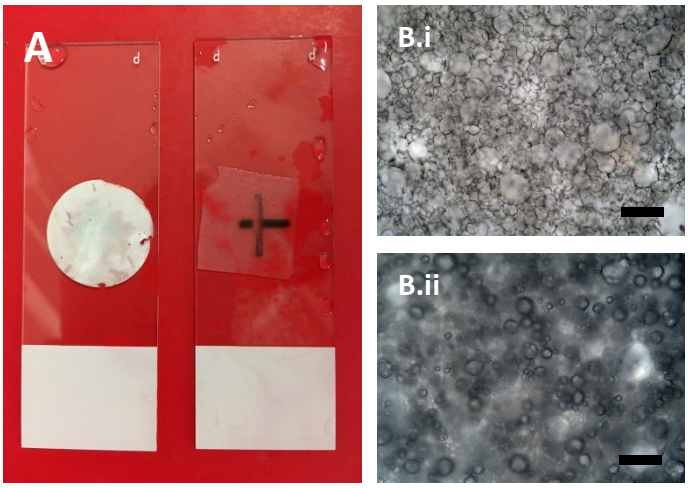

Figure 4. TMPTA (left) and PEGDA (right) polyHIPE materials swollen in water and placed on a glass microscope slide. Black cross on the back of the slide to demonstrate transparency (**A**). Bright field microscope images taken at x20 magnification and identical exposure times of PEGDA (**i**) and TMPTA (**ii**) polyHIPE materials swollen in water (**B**) (Scale bars = 100 µm).

Mechanical Testing

Tensile testing to ASTMD638 standards was used to determine mechanical properties of polyHIPE materials. PolyHIPE samples were produced as sheets of approximately 3 mm thickness, from which dog bone-shaped samples were stamped out using an ASTMD638 Type V die. All four materials were first tested in a completely dry state. Samples were extended uniaxially at a constant rate of 10 mm/min until break. All samples exhibited non-linear j-shaped stress-strain curves, typical of polymeric foams[61] and other biomaterials.[62] Strain at break, stress at break and

elastic modulus were obtained from the plots of stress vs. strain (**Table 1**). The TMPTA materials gave the highest elastic modulus at 68 kPa, a slightly lower value than previously reported.[39] As hypothesised, substituting the trifunctional crosslinker for a difunctional crosslinker produced a significant reduction in the elastic modulus from 68 to 27 kPa. Interestingly, the strain at break increased, most likely due to added flexibility in the polymer network caused by the reduction in the degree of crosslinking. The introduction of a longer, PEG-based, difunctional crosslinker gave no significant reduction in elastic modulus at the same porosity value, but did however produce a large increase in both stress and stain at break compared to the HDDA-crosslinked material. Again, this is most likely due to the added flexibility in the polymer network, this time brought about by a longer difunctional crosslinker which increases the chain length between crosslinks. Increasing the porosity of the PEGDA polyHIPE from 80 to 85% produced no significant change in the strain at break, but did however give a drop in the stress at break to 99 kPa and, more importantly, a drop in the elastic modulus to 13 kPa. As previously mentioned, the elastic modulus of the mammalian brain has been reported as being in the range of 0.1 – 24 kPa; the elastic modulus of the 85% porous PEGDA polyHIPE in the dry state lies in this range.

Table 1. Mechanical properties of polyHIPE materials in their dry state[a]

	Strain at Break (%)	Stress at Break (kPa)	Elastic Modulus (kPa)
TMPTA_80%	250±8.6	220±15	68±1.7
HDDA_80%	290±66	100±28	27±3.2
PEGDA_80%	730±60	220±21	24±1.1
PEGDA_85%	620±52	99±12	13±0.6

[a] N=6, mean±standard deviation

Due to the extensive swelling of the PEGDA-based polyHIPEs, tensile testing was also performed in PBS at 37°C to mimic *in vivo* conditions. Due to the extension limitations of the apparatus, tests could not be performed to break. Only elastic modulus values were obtained from the stress-strain data. Samples again were produced as sheets of approximately 3 mm thick. Sheets were immersed in PBS for 24 hours to reach equilibrium swelling. Dog bone samples were then stamped out of the swollen sheet using an ASTMD638 Type V die.

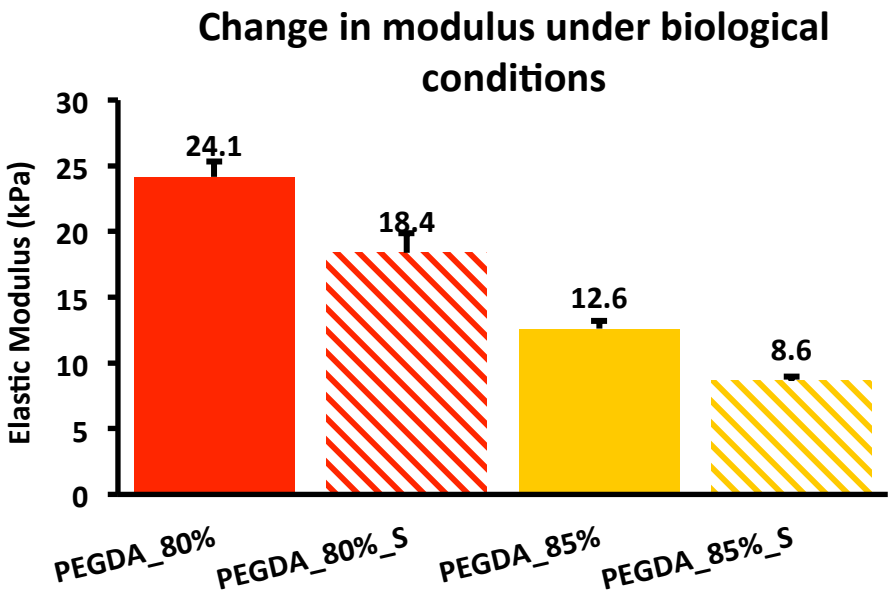

Figure 5. Comparison of elastic modulus of PEGDA based polyHIPEs under dry conditions and mimicked biological conditions swollen (S) in PBS at 37°C (N=6, mean ± standard deviation)

A significant reduction in modulus was observed for both 80 and 85% porous PEGDA polyHIPE materials when tested swollen under mimicked biological conditions (**Figure 5**). When swollen, a given volume of PEGDA polyHIPE contains less polymeric material then the same given volume in the dry state. This reduction in material is most likely the reason as to why the modulus was

shown to decrease in the swollen state. Both 80 and 85% PEGDA materials in the swollen state display elastic modulus values in the range reported for that of mammalian brain tissue at 18.4 and 8.6 kPa respectively. These two materials display ideal mechanical properties for use as scaffolds for mammalian neural tissue engineering.

Degradation Studies

A tissue engineering scaffold's ability to degrade in a timely manner and allow normal tissue ECM synthesis to take over can greatly enhance its ability to produce tissue that more accurately represents that found *in vivo*. It was hypothesised that these thiol-ene materials could degrade via ester hydrolysis. Materials were placed in PBS at 37°C and their change in mass over time was determined (**Figure 6A**). Materials were also placed in 0.1 M NaOH at room temperature to accelerate the ester hydrolysis degradation process (**Figure 6B**).

The 80% porous PEGDA crosslinked material was shown to degrade at the fastest rate under both mimicked biological and accelerated conditions. This is most likely due to the high affinity to water of the material, attracting water and increasing its access to the ester groups. The HDDA material degraded slower than the PEDGA material, but faster than the TMPTA material under accelerated conditions. Despite having the same concentration of ester linkages as the TMPTA material, the HDDA material in theory has a lower cross-link density giving it less impeded access for water to attack the ester groups. The TMPTA material displayed a significantly slower degradation rate than both the HDDA and PEGDA materials under accelerated conditions. The TMPTA material is the least liable to hydrolytic degradation as it has a hydrophobic crosslinker and in theory has the highest cross-link density of the materials.

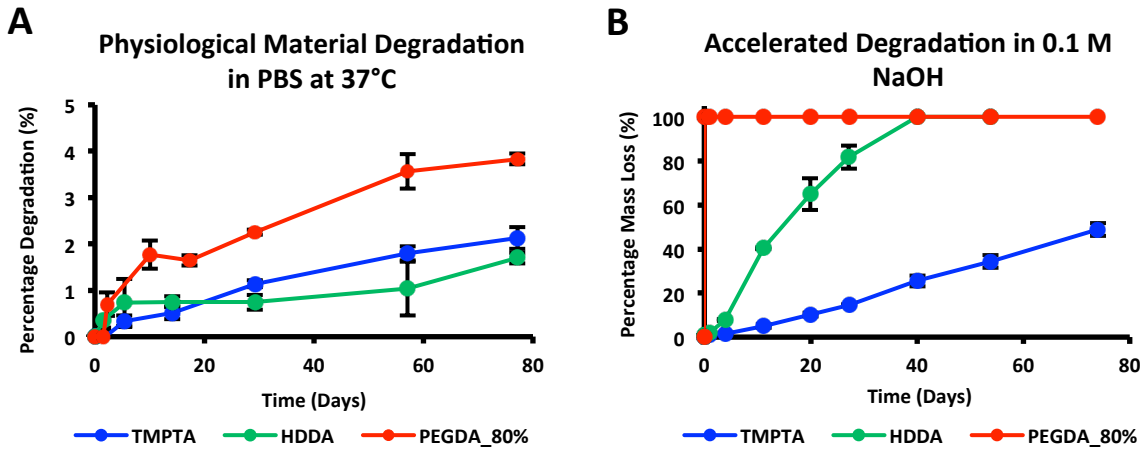

Figure 6. Materials degradation experiments. Degradation under mimicked physiological conditions in PBS at 37°C (**A**) and under accelerated conditions in 0.1M NaOH at room temperature (**B**). (N=3, mean ± standard deviation)

Under mimicked biological conditions all materials exhibited slow degradation profiles. After 77 days immersion in PBS at 37°C, PEGDA_80%, HDDA and TMPTA materials exhibited only 2.1, 1.7 and 3.8% mass loss. The PEGDA_80% material showed the greatest degradation rate. There was no significant difference between the degradation rate of the HDDA and TMPTA materials. The PEGDA_80% material displayed rapid degradation in the 0.1 M NaOH solution. The material was seen to be fully solubilised within 30 minutes of immersion in the basic solution. The HDDA material was the next fastest to fully degrade, and was shown to completely degrade after 40 days under accelerated conditions. After 74 days under accelerated conditions the TMPTA was slowest to degrade with a percentage mass loss of 52%.

3D Human Neural Progenitor Cell Culture

Human HDF51i509 iPSC-derived NPCs were transferred from validated expansion cultures on 2D laminin-coated tissue culture polystyrene (TCPS) (**Figure 7A-B**) to test cultures on all four scaffold

materials (TMPTA, HDDA, PEGDA_80%, PEGDA_85%) as well as on Alvetex®, a control scaffold purchased from ReproCELL, all coated in 10 µg/mL laminin. Scaffolds were each seeded with $1x10^6$ hNPCs (per scaffold disk) and cultured for 3 days.

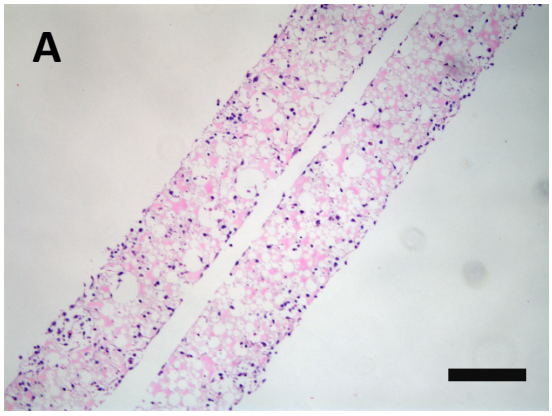

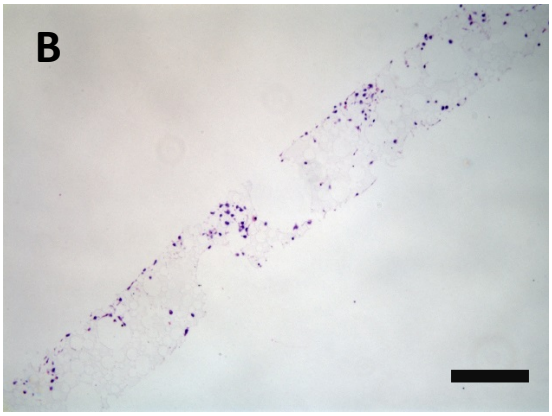

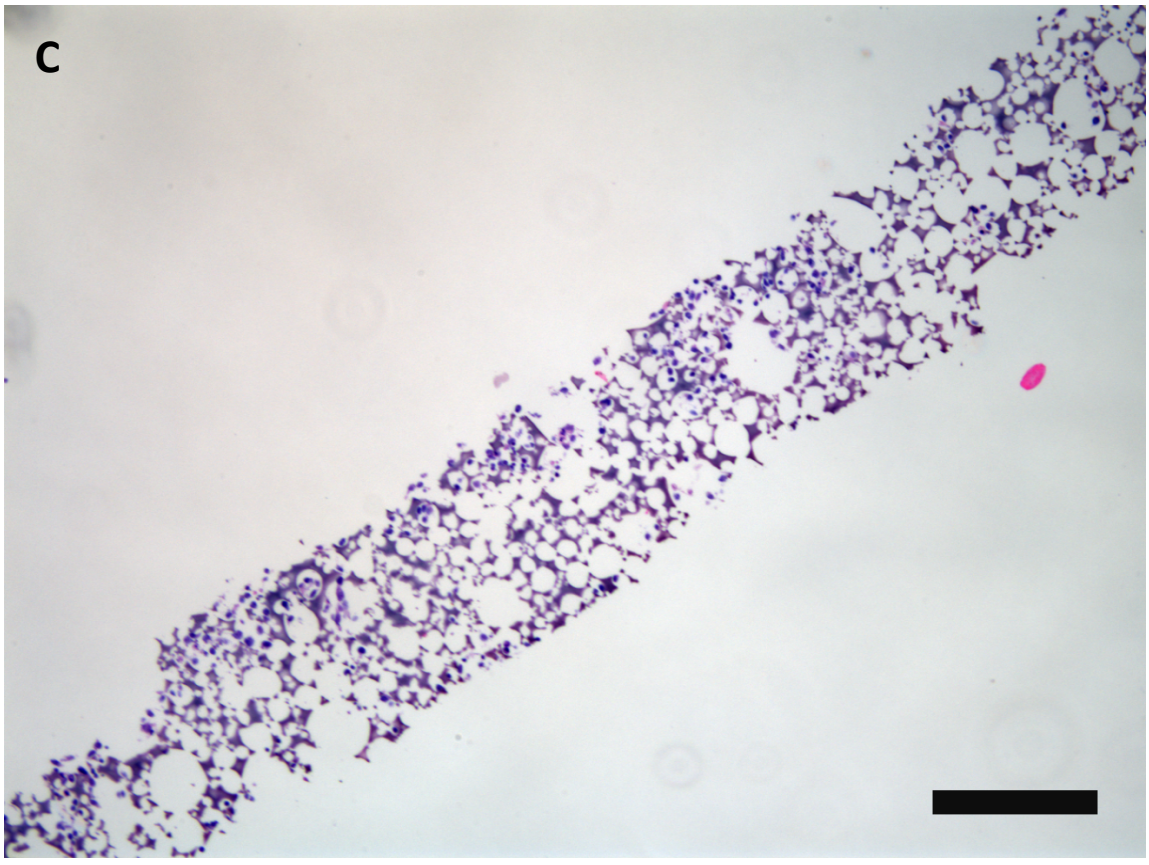

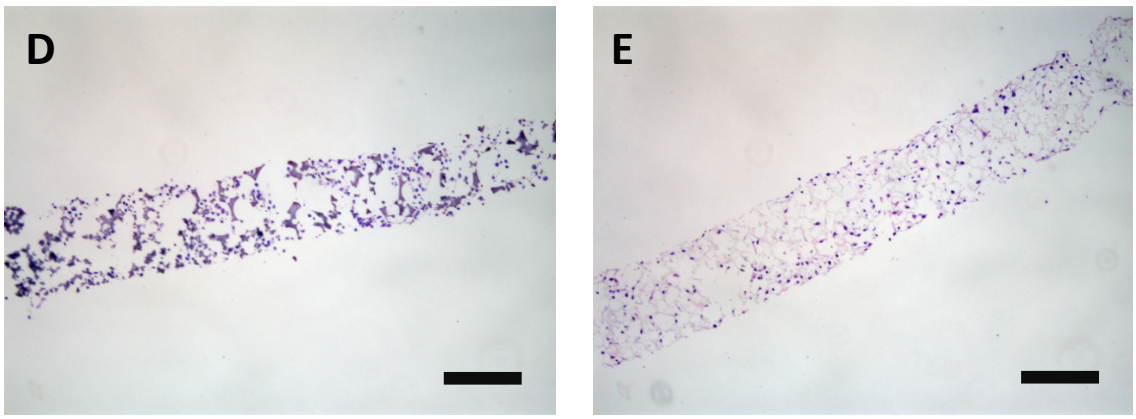

Figure 7. HDF51i509 hNPCs (passage 18) seeded at 1x10^6 cells/scaffold and cultured for 3 days on laminin-coated scaffold materials TMPTA (**A**), HDDA (**B**), PEGDA_85% (**C**), PEGDA_80% (**D**) and Alvetex® control (**E**) stained with hematoxylin and eosin. (Scale bar = 200 µm)

By H&E staining, NPCs were observed to be distributed throughout each of the five materials (**Figure 7A-E**). All sections of polyHIPE materials displayed cell densities comparable to that for the commercially available Alvetex® scaffold, which has demonstrated biocompatibility with a wide range of cell types. HNPCs appear to be distributed throughout all materials, and do not appear to be residing on the top and bottom surfaces of any materials. The hematoxylin (dark purple) seems to stain strongly the hydrophilic PEGDA materials, making it slightly more difficult to visualise the hNPCs (**Figure 7C** and **D**). Interestingly, the eosin counterstain (light purple) seems to have stained the TMPTA scaffold material. These results indicate potential for these materials as scaffolds for longer term 3D human neural progenitor cell culture studies.

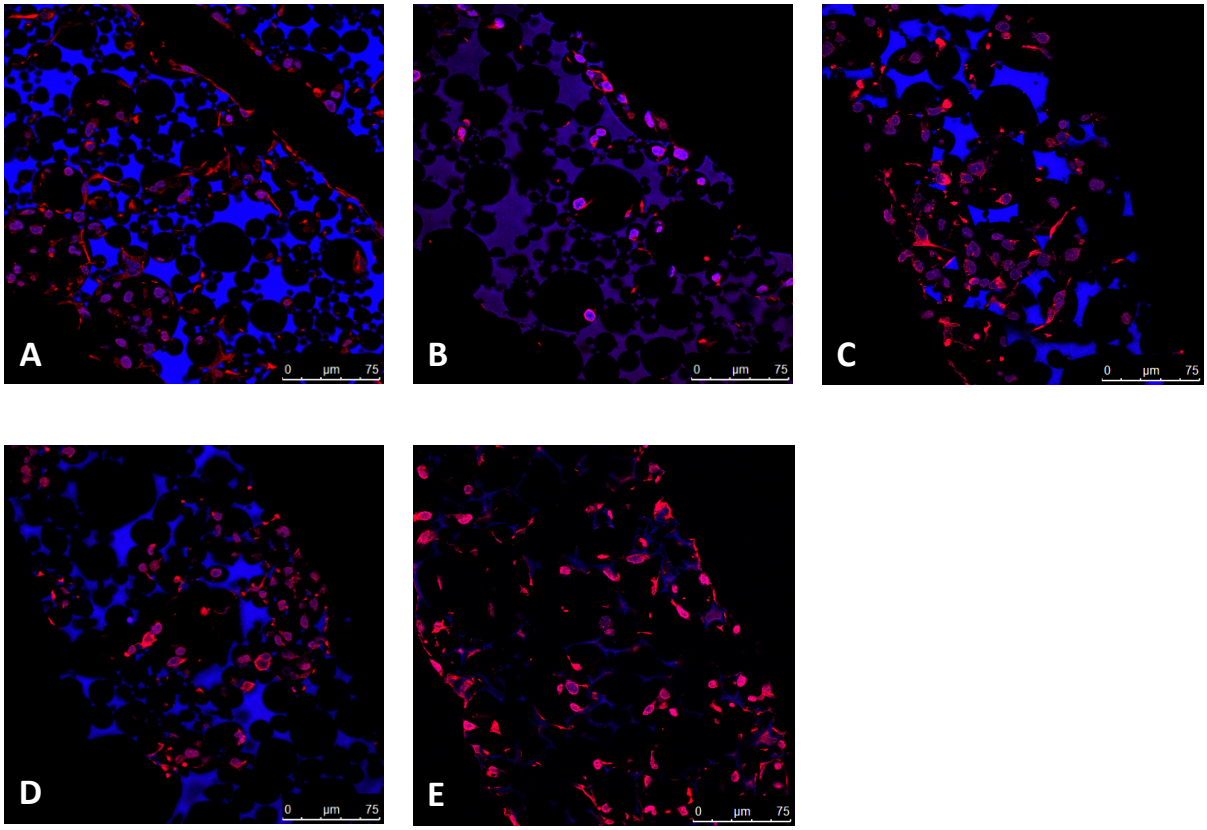

Figure 8. HDF51i509 hNPCs (passage 18) seeded at 1x10^6 cells/scaffold and cultured for 3 days on laminin-coated scaffolds, PFA-fixed and immunostained with 3CB2 anti-vimentin, detected by Alex Fluor 568 (red). Cell nuclei are counterstained with DAPI (blue). TMPTA (**A**), HDDA (**B**), PEGDA_80% (**C**), PEGDA_85% (**D**) and Alvetex control (**E**). Mouse IgM isotype and goat anti-mouse IgM AF568 controls in Supplementary Information.

To demonstrate a phenotypic identity for the iPSC-derived hNPCs cultured within these scaffold materials, cells were immunostained to detect the expression of vimentin, a type III intermediate filament protein[63] that contributes to the filamentous network of the cell cytoskeleton.[64] Vimentin is found in the radial glial cells that arise from the primitive neuroepithelial lineage of the developing CNS and give rise both *in vivo* and *in vitro* from the early differentiation of hPSCs to neurons, astrocytes and oligodendrocytes.[65, 66] HNPCs cultured on all materials were shown to

stain positive for the detection of vimentin protein (**Figure 8A-E**), indicative of retaining their radial glial-like state and multipotent phenotype after transfer from 2D expansion culture to short term 3D scaffold cultures. Background blue staining arises from scaffold autofluorescence in the blue channel (**Figure S3**). All scaffold materials display potential for longer term cultures to support the growth and differentiation of hNPCs to neuronal and glial cell types which could have potential applications for *in vitro* disease modelling.

Conclusions

The work presented here describes the synthesis of a novel porous polymeric material tailor-made for neural tissue engineering. The material, synthesised with a poly(ethylene glycol) diacrylate crosslinker, has an elastic modulus of 9 kPa, similar to values reported for that of mammalian brain tissue. The material is also shown to absorb up to 7 times more cell culture medium than previous emulsion-templated tissue engineering scaffolds. PEGDA_80% materials were also shown to have significantly improved light transmission abilities, beneficial for cell culture imaging. PEGDA_80% materials showed 3.8% degradation after 11 week incubation in mimicked biological conditions. The same material also displayed full degradation under accelerated conditions in 0.1 M NaOH after 30 minutes. After 3 days culture with iPSC-derived human neural progenitor cells, all materials presented in this work displayed the presence of hNPCs that appear to have migrated throughout the scaffold. HNPCs within the scaffold materials were also shown to retain expression of the protein vimentin, indicative of the materials supporting the viable culture of human cells with a radial glial-like phenotype. Both 80 and 85% porous PEGDA crosslinked materials show great promise as neural tissue engineering scaffolds due to the combination of a favourable environment for hNPC culture and elastic modulus values close to that of mammalian brain tissue.

Conflicts of Interest

There are no conflicts to declare.

Acknowledgements

The authors acknowledge the use of facilities and technical assistance of Monash Histology Platform, Department of Anatomy and Developmental Biology; and of Monash Micro Imaging, Monash University, Victoria, Australia. HPSC-NPC derivation research (IG, JP, ALL, CO'B) was supported by California Institute for Regenerative Medicine (CIRM) joint grant funding (TR3-05603) with Australia's NHMRC (to CO'B, ALL).

References

1. W. K. Raja, A. E. Mungenast, Y. T. Lin, T. Ko, F. Abdurrob, J. Seo and L. H. Tsai, *PloS One*, 2016, **11**, e0161969.
2. E. Carletti, A. Motta and C. Migliaresi, in *3D Cell Culture: Methods and Protocols*, ed. J. W. Haycock, Humana Press, Totowa, NJ, p. 17.
3. C. D'Avanzo, J. Aronson, Y. H. Kim, S. H. Choi, R. E. Tanzi and D. Y. Kim, *Bioessays*, 2015, **37**, 1139-1148.
4. B. De Strooper, *Cell*, 2014, **159**, 721-726.
5. B. P. Chan and K. W. Leong, *Eur. Spine J.*, 2008, **17 Suppl 4**, 467-479.
6. F. J. O'Brien, *Mater. Today*, 2011, **14**, 88-95.
7. D. L. Jones and A. J. Wagers, *Nat. Rev. Mol. Cell Biol.*, 2008, **9**, 11-21.
8. P. A. Riquelme, E. Drapeau and F. Doetsch, *Philos. T. Roy. Soc. B*, 2008, **363**, 123-137.

9. E. Ruoslati, *Glycobiology*, 1996, **6**, 489-492.

10. L. W. Lau, R. Cua, M. B. Keough, S. Haylock-Jacobs and V. W. Yong, *Nat. Rev. Neurosci.*, 2013, **14**, 722-729.

11. M. P. Lutolf and H. M. Blau, *Adv. Mater.*, 2009, **21**, 3255-3268.

12. J. A. Thomson, J. Itskovitz-Eldor, S. S. Shapiro, M. A. Waknitz, J. J. Swiergiel, V. S. Marshall and J. M. Jones, *Science*, 1998, **282**, 1145-1147.

13. K. Takahashi, K. Tanabe, M. Ohnuki, M. Narita, T. Ichisaka, K. Tomoda and S. Yamanaka, *Cell*, 2007, **131**, 861-872.

14. L. Gerrard, L. Rodgers and W. Cui, *Stem Cells*, 2005, **23**, 1234-1241.

15. P. Itsykson, N. Ilouz, T. Turetsky, R. S. Goldstein, M. F. Pera, I. Fishbein, M. Segal and B. E. Reubinoff, *Mol. Cell. Neurosci.*, 2005, **30**, 24-36.

16. M. F. Pera, J. Andrade, S. Houssami, B. Reubinoff, A. Trounson, E. G. Stanley, D. Ward-van Oostwaard and C. Mummery, *J. Cell Sci.*, 2004, **117**, 1269-1280.

17. S. M. Chambers, C. A. Fasano, E. P. Papapetrou, M. Tomishima, M. Sadelain and L. Studer, *Nat. Biotechnol.*, 2009, **27**, 275-280.

18. A. Tamura, S. Hayashi, I. Watanabe, K. Nagayama and T. Matsumoto, *J. Biomech. Sci. Eng.*, 2007, **2**, 115-126.

19. G. T. Fallenstein, V. D. Hulce and J. W. Melvin, *J. Biomech.*, 1969, **2**, 217-226.

20. B. S. Elkin, E. U. Azeloglu, K. D. Costa and B. Morrison, 3rd, *J. Neurotrauma*, 2007, **24**, 812-822.

21. A. Gefen, N. Gefen, Q. Zhu, R. Raghupathi and S. S. Margulies, *J. Neurotrauma*, 2003, **20**, 1163-1177.

22. E. R. Aurand, J. Wagner, C. Lanning and K. B. Bjugstad, *J. Funct. Biomater.*, 2012, **3**, 839-863.

23. W. J. Tyler, *Nat. Rev. Neurosci.*, 2012, **13**, 867-878.

24. S. Ali, I. B. Wall, C. Mason, A. E. Pelling and F. S. Veraitch, *Acta Biomater.*, 2015, **25**, 253-267.

25. A. Banerjee, M. Arha, S. Choudhary, R. S. Ashton, S. R. Bhatia, D. V. Schaffer and R. S. Kane, *Biomaterials*, 2009, **30**, 4695-4699.

26. N. D. Leipzig and M. S. Shoichet, *Biomaterials*, 2009, **30**, 6867-6878.

27. K. Saha, A. J. Keung, E. F. Irwin, Y. Li, L. Little, D. V. Schaffer and K. E. Healy, *Biophys. J.*, 2008, **95**, 4426-4438.

28. T. Garg and A. K. Goyal, *Expert Opin. Drug Deliv.*, 2014, **11**, 767-789.

29. M. W. Hayman, K. H. Smith, N. R. Cameron and S. A. Przyborski, *J. Biochem. Biophys. Methods*, 2005, **62**, 231-240.

30. E. Rossi, I. Gerges, A. Tocchio, M. Tamplenizza, P. Aprile, C. Recordati, F. Martello, I. Martin, P. Milani and C. Lenardi, *Biomaterials*, 2016, **104**, 65-77.

31. K. Seunarine, N. Gadegaard, M. Tormen, D. O. Meredith, M. O. Riehle and C. D. W. Wilkinson, *Nanomedicine*, 2006, **1**, 281-296.

32. B. Dhandayuthapani, Y. Yoshida, T. Maekawa and D. S. Kumar, *Int. J. Polym. Sci.*, 2011, **2011**, 1-19.

33. W. Busby, N. R. Cameron and C. A. Jahoda, *Biomacromolecules*, 2001, **2**, 154-164.

34. W. Busby, N. R. Cameron and A. B. C. Jahoda, *Polym. Int.*, 2002, **51**, 871-881.

35. M. Bokhari, M. Birch and G. Akay, *Adv. Exper. Med. Biol.*, 2003, **534**, 247-254.

36. A. Barbetta, M. Dentini, E. M. Zannoni and M. E. De Stefano, *Langmuir*, 2005, **21**, 12333-12341.

37. E. M. Christenson, W. Soofi, J. L. Holm, N. R. Cameron and A. G. Mikos, *Biomacromolecules*, 2007, **8**, 3806-3814.

38. R. S. Moglia, J. L. Holm, N. A. Sears, C. J. Wilson, D. M. Harrison and E. Cosgriff-Hernandez, *Biomacromolecules*, 2011, **12**, 3621-3628.

39. S. Caldwell, D. W. Johnson, M. P. Didsbury, B. A. Murray, J. J. Wu, S. A. Przyborski and N. R. Cameron, *Soft Matter*, 2012, **8**, 10344.

40. J. L. Robinson, R. S. Moglia, M. C. Stuebben, M. A. P. McEnery and E. Cosgriff-Hernandez, *Tissue Eng. Part A*, 2014, **20**, 1103-1112.

41. J. Naranda, M. Susec, U. Maver, L. Gradisnik, M. Gorenjak, A. Vukasovic, A. Ivkovic, M. S. Rupnik, M. Vogrin and P. Krajnc, *Sci. Rep.*, 2016, **6**, 28695.

42. R. Owen, C. Sherborne, T. Paterson, N. H. Green, G. C. Reilly and F. Claeyssens, *J. Mech. Behav. Biomed. Mater.*, 2016, **54**, 159-172.

43. J. L. Robinson, M. A. McEnery, H. Pearce, M. E. Whitely, D. J. Munoz-Pinto, M. S. Hahn, H. Li, N. A. Sears and E. Cosgriff-Hernandez, *Tissue Eng. Part A*, 2016, **22**, 403-414.

44. A.-J. Wang, T. Paterson, R. Owen, C. Sherborne, J. Dugan, J.-M. Li and F. Claeyssens, *Mater. Sci. Eng. C-Mater. Biol. Appl.*, 2016, **67**, 51-58.

45. S. D. Kimmins and N. R. Cameron, *Adv. Funct. Mater.*, 2011, **21**, 211-225.

46. I. Pulko and P. Krajnc, *Macromol. Rapid Commun.*, 2012, **33**, 1731-1746.

47. M. S. Silverstein, *Polymer*, 2014, **55**, 304-320.

48. P. Becher, *J. Disper. Sci. Technol.*, 1985, **6**, 147.

49. E. Lovelady, S. D. Kimmins, J. Wu and N. R. Cameron, *Polym. Chem.*, 2011, **2**, 559-562.

50. M. Turnsek and P. Krajnc, *Macromol. Chem. Phys.*, 2013, **214**, 2528-2533.

51. C. R. Langford, D. W. Johnson and N. R. Cameron, *Polym. Chem.*, 2014, **5**, 6200-6206.

52. A. Barbetta and N. R. Cameron, *Macromolecules*, 2004, **37**, 3188-3201.

53. K. Kendall and K. N. G. Fuller, *J. Phys. D: Appl. Phys*, 1987, **20**, 1596-1600.

54. J. C. Jones, K. Sabatini, X. Liao, H. T. Tran, C. L. Lynch, R. E. Morey, V. Glenn-Pratola, F. S. Boscolo, Q. Yang, M. M. Parast, Y. Liu, S. E. Peterson, L. C. Laurent, J. F. Loring and Y. C. Wang, *J. Invest. Dermatol.*, 2013, **133**, 2104-2108.

55. J. Beers, D. R. Gulbranson, N. George, L. I. Siniscalchi, J. Jones, J. A. Thomson and G. Chen, *Nat. Protoc.*, 2012, **7**, 2029-2040.

56. J. Itskovitz-Eldor, M. Schuldiner, D. Karsenti, A. Eden, O. Yanuka, M. Amit, H. Soreq and N. Benvenisty, *Mol. Med.*, 2000, **6**, 88-95.

57. L. Conti, S. M. Pollard, T. Gorba, E. Reitano, M. Toselli, G. Biella, Y. Sun, S. Sanzone, Q. L. Ying, E. Cattaneo and A. Smith, *PLoS Biol.*, 2005, **3**, e283.

58. K. C. Sonntag, J. Pruszak, T. Yoshizaki, J. van Arensbergen, R. Sanchez-Pernaute and O. Isacson, *Stem Cells*, 2007, **25**, 411-418.

59. K. Watanabe, M. Ueno, D. Kamiya, A. Nishiyama, M. Matsumura, T. Wataya, J. B. Takahashi, S. Nishikawa, S. Nishikawa, K. Muguruma and Y. Sasai, *Nat. Biotechnol.*, 2007, **25**, 681-686.

60. I. Bruzauskaite, D. Bironaite, E. Bagdonas and E. Bernotiene, *Cytotechnology*, 2016, **68**, 355-369.

61. N. J. Mills, *Polymer Foams Handbook: Engineering and Biomechanics Applications and Design Guide*, Butterworth-Heinemann, Oxford, 2007.

62. G. A. Holzapfel, in *The Handbook of Materials Behavior Models*, ed. J. Lemaitre, Academic Press, San Diego, CA, 2001, vol. 3, pp. 1057-1071.

63. E. Fuchs and K. Weber, *Annu. Rev. Biochem.*, 1994, **63**, 345-382.

64. M. J. Perez-Alvarez, C. Isiegas, C. Santano, J. J. Salazar, A. I. Ramirez, A. Trivino, J. M. Ramirez, J. P. Albar, E. J. de la Rosa and C. Prada, *J. Neurosci. Res.*, 2008, **86**, 1871-1883.

65. M. Gotz and Y. A. Barde, *Neuron*, 2005, **46**, 369-372.

66. M. Sild and E. S. Ruthazer, *Neuroscientist*, 2011, **17**, 288-302.